


ARTICLE

Open Access

A novel function of *IMPA2*, plays a tumor-promoting role in cervical cancer

Kan Zhang¹, Lei Liu¹, Min Wang¹ , Min Yang¹, Xianping Li¹, Xiaomeng Xia², Jingjing Tian¹, Shan Tan¹ and Lingli Luo¹

Abstract

Discovery of genes and molecular mechanism involved in cervical cancer development would promote the prevention and treatment. By comparing gene expression profiles of cervical carcinoma in situ (CCIS) and adjacent normal tissues, we identified a potential cancer-promoting gene, *IMPA2*. This study aimed to elucidate the role of *IMPA2* and underlying molecular mechanisms in cervical cancer progression. To do this expression of *IMPA2* was compared between human cervical cancer and corresponding adjacent normal cervical tissues firstly. CCK-8 assay, clone formation assay, wound healing assay, transwell assay, and tumor formation in nude mice were performed to demonstrate the effect of *IMPA2* in cervical cancer proliferation and metastasis. Further proteomic profiling and western blotting explored the molecular pathway involved in the *IMPA2*-regulating process. The results showed that *IMPA2* gene expression was upregulated in cervical cancer. Consistently, silencing of *IMPA2* suppressed tumor formation in BALB/c nude mice. Short hairpin RNA (shRNA)-mediated *IMPA2* silencing significantly inhibited proliferation and colony-forming abilities of cervical cancer cells, while *IMPA2* overexpression had little impact. Also, *IMPA2* silencing suppressed cellular migration, but overexpression promoted migration. Proteomics analysis revealed the involvement of mitogen-activated protein kinase (MAPK) pathway in tumor-promoting action of *IMPA2*. Significantly, the inhibition of *IMPA2* activated ERK phosphorylation, and its inhibitory effects can be restored by using selective ERK inhibitor, FR180204. In conclusion, *IMPA2* acts as an oncogene in the proliferation and migration of cervical cancer. *IMPA2* downregulated ERK phosphorylation to promote cervical cancer. These findings identify a new mechanism underlying cervical cancer and suggest a regulating effect of *IMPA2* in MAPK signaling pathway.

Introduction

Cervical cancer is the fourth leading cause of cancer-associated death regarding gynecological malignancies worldwide¹, even though prevention and treatment have rapidly developed recently^{2,3}. As we all know, the most significant cause of cervical cancer is persistent infection of human papillomavirus (HPV). HPV is detected in 99% of cervical cancer patients⁴, but most women infected with HPV failed to develop invasive cervical cancer⁵. Therefore, comprehensive understanding of molecular

mechanisms underlying cervical cancer will promote the earlier diagnosis and effective treatment.

Genetic mutations were proved to play important roles in development of cervical cancer⁶. RNA sequencing provides an efficient and comprehensive method to identify the key genes and molecular pathways involved in cervical cancer pathogenesis^{7,8}. Cervical carcinoma in situ (CCIS), without stromal invasion, and superficially invasive carcinomatosis, is the earliest stage in cancer progression. By comparing gene expression profiles of CCIS and adjacent normal tissues, it is possible to look for the most direct evidence of tumorigenesis and help early diagnosis. Here, we sought potential oncogenes of cervical cancer, by comparing mRNA expression profiles of tissue samples of CCIS with adjacent normal cervical tissue. *IMPA2* gene was discovered to be significantly upregulated in CCIS tissues. *IMPA2* located on chromosome

Correspondence: Min Wang (wangmin0000@csu.edu.cn)

¹Department of Laboratory Medicine, Second Xiangya Hospital, Central South University, Changsha, Hunan, China

²Department of Obstetrics and Gynecology, Second Xiangya Hospital, Central South University, Changsha, Hunan, China

These authors contributed equally: Kan Zhang, Lei Liu
Edited by J.-E. Ricci

© The Author(s) 2020



Open Access This article is licensed under a Creative Commons Attribution 4.0 International License, which permits use, sharing, adaptation, distribution and reproduction in any medium or format, as long as you give appropriate credit to the original author(s) and the source, provide a link to the Creative Commons license, and indicate if changes were made. The images or other third party material in this article are included in the article's Creative Commons license, unless indicated otherwise in a credit line to the material. If material is not included in the article's Creative Commons license and your intended use is not permitted by statutory regulation or exceeds the permitted use, you will need to obtain permission directly from the copyright holder. To view a copy of this license, visit <http://creativecommons.org/licenses/by/4.0/>.

Table 1 Clinical characteristic of cervical cancer patients enrolled in this study.

ID	Age at diagnosis (years)	Pathological type	FIGO stage	HPV types	Reproductive history (pregnancy-birth-abortion)
1	47	CIS	0	51+/52+/44+	5-1-4
2	51	CIS	0	33+/53+	5-2-3
3	43	CIS	0	16+/53+	2-1-1

CIS carcinoma in situ, FIGO International Federation of Gynecology and Obstetrics, HPV Human Papilloma Virus.

18p11.2, encodes myo-inositol monophosphatase 2 (IMPA2) with 288 amino acids⁹. IMPA2 has intrinsic IMPase activity that is completely dependent on magnesium¹⁰, and is involved in phosphatidylinositol signaling pathway, which is associated with cellular activities such as metabolism, secretion, cell growth, and differentiation¹¹. Therefore, we speculated that *IMPA2* may be a cancer-promoting gene in cervical cancer. However, most studies about *IMPA2* focused on neuropsychiatric diseases and the pharmacological action of Lithium^{10,12,13}. Recently, French et al.¹⁴ found that *IMPA2* expression might affect accumulation of methotrexate polyglutamates (MTXPGs) in leukemia. In addition, Lin et al.¹⁵ indicated that *IMPA2* downregulation leads to poor outcomes in clear cell renal cell carcinoma (ccRCC). This is contrary to our speculation on the role of *IMPA2* in cervical cancers. As there are few published articles about the role of *IMPA2* gene in cervical cancer, this study performed both in vitro and in vivo studies to discuss the relationship between cervical cancer and *IMPA2*.

Here, we discussed the role of *IMPA2* and found that *IMPA2* promoted the ability of proliferation, metastasis, and in vivo tumorigenesis of cervical cancer cells. Further proteomic analysis was performed to discuss the possible mechanisms regulated by *IMPA2* in cervical cancer. The present study is proposed to identify the potential cancer-promoting action of *IMPA2* in cervical cancer and explore possible pathways controlled by *IMPA2* to further understanding the molecular mechanisms underlying cervical cancer.

Material and methods

Tissue sample selection

Cervical carcinoma in situ (CCIS) and adjacent normal tissues were obtained from three patients who underwent radical hysterectomy at the Second Xiangya Hospital, Central South University. All patients were diagnosed by multipoint biopsy. Table 1 showed the clinical characteristics of the patients. After tumor purity analysis performed by ESTIMATE algorithm, samples were

collected for transcriptome analyses¹⁶. None of the three patients had received adjuvant therapy (chemotherapy or radiotherapy) prior to uterectomy. In addition, the other 58 patients with cervical cancer were enrolled from September 2015 to December 2017. Clinicopathologic features of the patients were shown in Table S1. Among them, 57.4% (35/61) were positive for HPV16, 19.7% (12/61) for HPV 58, 11.5% (7/61) for HPV 33, 11.5% (7/61) for HPV 52, 8.2% (5/61) for HPV51, and 8.2% (5/61) for HPV18. This study was approved by the Joint Ethics Committee of the Central South University Health Authority and performed following national guidelines. Written informed consent was obtained from all the patients. The clinical staging and clinicopathological classifications were determined according to the International Federation of Obstetrics and Gynecology (FIGO). Paired cervical cancer and adjacent normal tissues were collected at surgery, immediately frozen in liquid nitrogen and stored until total RNA or proteins were extracted.

Immunohistochemistry staining analysis

The immunohistochemical staining procedure was performed as previously described¹⁷. Cervical cancer samples for *IMPA2* detecting were obtained from the Second Xiangya Hospital of Central South University. Samples for ERK and p-ERK detecting were xenografts from mice. The staining positivity was determined by the following formula: IRS = intensityscore × quantity score. The percentage of positive cells was divided into five score ranks: <10% (0), 10–25% (1), 25–50% (2), 50–75% (3), and >75% (4). The intensity of staining was divided into four score ranks: no staining (0), light brown(1), brown (2), and dark brown (3). Two different pathologists evaluated all the specimens in a blinded manner. The antibodies used were as follows: anti-*IMPA2* rabbit monoclonal antibody (1:100, GeneCopoeis, USA); anti-ERK (1:500, Abcam, UK), and anti-pERK (1:400, Cell Signaling, USA).

Cell culture

Cervical cancer cell line SiHa (#BNCC337881) and normal cervical epithelial cell line, HcerEpic (#BNCC340373) were purchased from the Cell Bank of BeNa culture collection (Beijing, China). Cervical cancer cell line HeLa (#GCC-UT0002CS) was purchased from the Cell Bank of Genechem (Shanghai, China). The cell line was cultured in Dulbecco's modified eagle medium (DMEM) (Gibco, Grand Island, NY, USA) supplemented with 10% fetal bovine serum (FBS) (Gibco, Grand Island, NY, USA) and 1% antibiotics at 37 °C in an atmosphere containing 5% CO₂.

IMPA2 silencing

The short hairpin RNA (shRNA) targeting *IMPA2* mRNA (shIMPA2) and the negative control were

obtained from Ribobio (Guangzhou, China). Sequences of shIMPA2 were listed as follow: forward 5'-CCGG GCCTTACAGACGATTAAGTATCTCGAGATAGTTA ATCGTCTGAAGGCTTTTTG-3'; Reverse 5'-AATTC AAAAAGCCTTACAGACGATTAAGTATCTCGAGAT AGTTAATCGTCTGTAAGGC-3'. The lentivirus was packaged using GV115 vector, pHelper 1.0 vector and pHelper 2.0 vector, as well as Lipofectamine 2000 (Invitrogen, Carlsbad, CA, USA; Thermo Fisher Scientific) for the HEK293T cell and then collected after 48 h. The SiHa cell line was infected with lentivirus and polybrene (1:500; Shanghai Ji Kai Gene Chemical Technology Co., Ltd., Shanghai, China) according to the manufacturer's instructions. The expression change of *IMPA2* was determined by reverse-transcription polymerase chain reaction (RT-PCR) and Western blotting at 72 h after transfection.

In vivo tumor formation assay

A total of 14 health female BALB/c (nu/nu) nudes (4 weeks, 20–23 g) were purchased from Shanghai Lingchang Biotechnology limited company and fed in SPF Animal Laboratory of Central South University with sterile water and food. The mice were divided into 2 groups based on the randomized table, Normal Control (shCtrl) group and *IMPA2* RNAi (shIMPA2) group. In all, 5×10^6 indicated stable cell lines were subcutaneously injected into right flank of BALB/c (nu/nu) mice in each group. Tumor sizes and weights were measured once a week. Mice were examined by in vivo fluorescence imaging system (Lumina LT, Perkin Elmer, USA) and killed for the analysis of tumor burden after 4 weeks. The tumors were stripped for follow-up experiments. All the experiments were strictly accordant with the care and use guidelines of experimental animal and approved by the Animal Protection Committee.

RNA isolation and quantitative real-time PCR

Total RNA was extracted using the Trizol reagent (Sangon Biotech, Shanghai, China). RNA (1 μ g) was reverse transcribed into cDNA using Transcriptor First Strand cDNA Synthesis Kit (Roche Diagnostics, Germany) according to the supplier's instructions. Quantitative real-time PCR analysis was performed with Stratagene Mx3000P qPCR system (Agilent Technologies, USA) using Thunderbird qPCR Mix (TOYOBO, Japan). CDNA samples were tested in triplicate and glyceraldehyde-3-phosphate dehydrogenase (GADPH) was used as a reference gene. The expression of *IMPA2* was quantified by measuring Ct values and normalized using the $2^{-\Delta\Delta Ct}$ method relative to GAPDH. The primer pairs used for qRT-PCR were designed using the primer3 program. Primers used were as follows: *IMPA2* forward, 5'-GAAACCTCTCTCGCAACTCAG-3', reverse, 5'-GGG

CAGGACAGATCATCAGAA-3'. GAPDH forward: 5'-GAACGGGAAGCT CACTGG-3', reverse, 5'-GCCTGC TTCACCACCT TCT-3'.

Western blotting analysis

Details of Western blotting were previously described¹⁸. Cells at 80–90% confluence were lysed on ice in radioimmunoprecipitation assay buffer (RIPA; keygen biotech, China) containing PMFS complete protease inhibitor cocktail (keygen biotech, China). Protein concentration was determined by the BCA assay (keygen biotech, China). Equal protein samples (10 μ g) were separated on 12% sodium dodecyl sulfate (SDS)/polyacrylamide gels, and transferred onto 0.45 μ m polyvinylidene difluoride (PVDF) membranes (Immobilon-P; Millipore, Bedford, MA, USA). The antibodies used were as follow: anti-*IMPA2* rabbit monoclonal antibody (1:1000; GeneCopeis, USA); anti-ERK (1:10,000, Abcam, UK), anti-p38 α (1:500, BBI China), anti-JNK1/2/3 (1:500, BBI China), p-ERK (1:500, Cell Signaling, USA), p-p38 α (p-Thr180/Tyr182, 1:500, BBI China), and p-JNK1/2/3 (p-Thr183/Tyr185, 1:500, BBI China). Horseradish peroxidase (HRP)-conjugated goat anti-rabbit immunoglobulin G (1:1000; BBI China) was used as second antibody and anti-GAPDH mouse monoclonal antibody (1:5000; BBI China) as a loading control. The final protein expression was detected by enhanced chemiluminescence (Bio-rad, Berkeley, CA, USA) according to the manufacturer's suggested protocols. The band quantification was conducted using ImageJ (National Institutes of Health, Bethesda, MA, USA).

CCK-8 cell viability assays

Cells were seeded into a 96-well plate at 2×10^3 cells per well with 100 μ l cultured medium and cultured for 24, 48, 72, and 96 h at 37 $^{\circ}$ C, 5% CO₂. The cell viability was determined with CCK8 assay as previously described¹⁹. Each process was repeated three times.

Colony formation assay

Cells (1000/well) were plated in 6-well plates and cultured for 2 weeks. The colonies were washed with PBS three times and fixed with 4% formaldehyde for 10 min. Then, the colonies were stained with 1% crystal violet for 10 min. After washing, the colonies were counted. The experiment was carried out in triplicate for each cell line.

Wound healing and transwell migration assays

In the wound healing assay, cells (2×10^6 /well) were seeded in 6-well plates. When the cells were 90% confluent, they were serum-starved for 24 h. A linear wound was created in the confluent monolayer using a 10- μ l pipette tip. The wounds were observed and photographed immediately (time 0) and thereafter at 48

(magnification, $\times 200$). Details of transwell migration assay was described previously²⁰, 2×10^4 cells in 200 μ l of serum-free medium were added to the top chamber of the transwell (8- μ m pore size, BD Biosciences, New Jersey, USA). The bottom well contained growth medium with 20% FBS. After 24 h incubation at 37 °C, cells that had migrated to the lower face of the filters were fixed with 4% paraformaldehyde and stained with hematoxylin and finally counted under a magnification of $\times 200$ (10 random fields/well). Each experiment was repeated at least 3 times.

Sample preparation for proteomic measurement

The cultured cells were scraped and collected in 1.5 mL Eppendorf tubes. Then, samples were sonicated three times on ice using a high intensity ultrasonic processor (Scientz) in lysis buffer (8 M urea, 1% Protease Inhibitor Cocktail). The remaining debris was removed by centrifugation at 12,000 \times g at 4 °C for 10 min. Finally, the supernatant was collected and the protein concentration was determined with BCA kit. The protein solution was reduced with 5 mM dithiothreitol for 30 min at 56 °C and alkylated with 11 mM iodoacetamide for 15 min at room temperature in darkness. The protein sample was then diluted by adding 100 mM NH₄HCO₃ to urea concentration <2 M. Finally, trypsin was added at 1:50 trypsin-to-protein mass ratio for the first digestion overnight and 1:100 trypsin-to-protein mass ratio for a second 4-h-digestion.

LC-MS/MS analysis

The tryptic peptides were separated by an EASY-nLC 1000 UPLC system and then subjected to NSI source followed by tandem mass spectrometry (MS/MS) in Q Exactive TM Plus (Thermo) coupled online to the UPLC. The resulting MS/MS data were processed using Maxquant search engine (v.1.5.2.8). Tandem mass spectra were searched against SwissProt Human database concatenated with reverse decoy database. Trypsin/P was specified as cleavage enzyme allowing up to two missing cleavages. The mass tolerance for precursor ions was set as 20 ppm in First search and 5 ppm in Main search, and the mass tolerance for fragment ions was set as 0.02 Da. Carbamidomethyl on Cys was specified as fixed modification, and oxidation on Met was specified as variable modifications. False positive rate (FDR) was adjusted to <1% and minimum score for peptides was set >40.

Bioinformatics analysis of differentially expressed proteins

Firstly, protein ID of the differentially expressed proteins (DEPs) were converted to UniProt ID according to the UniProt-GOA database ([www. http://www.ebi.ac.uk/GOA/](http://www.ebi.ac.uk/GOA/)) and then mapped to Gene Ontology (GO) IDs. Proteins were classified by GO annotation based on three

categories: biological process, cellular component, and molecular function. Then, Kyoto Encyclopedia of Genes and Genomes (KEGG) database was used to annotate protein pathway and to identify enriched pathways. KEGG online service tools KAAS and KEGG mapper help annotate protein's KEGG database description and map the annotation result on the KEGG pathway database. Finally, a two-tailed Fisher's exact test were used to test the enrichment of the DEP against all identified proteins. A corrected *p*-value <0.05 was considered significant.

Statistical analysis

The results were analyzed using SPSS 22.0 (Chicago, IL, USA) and GraphPad Prism 6 software (GraphPad Software, San Diego, CA, USA). The data were expressed as the mean \pm SD. The *t*-test and one-way ANOVA Tukey's post-hoc test were used to analyze the statistical significance of parametric data from two and more independent samples, respectively. Non-parametric Wilcoxon Signed-Ranks test, Friedman test, Mann–Whitney *U* test and Kruskal–Wallis test were used to analyze data from two related samples, three or more related samples, two independent samples and three or more independent samples, respectively.

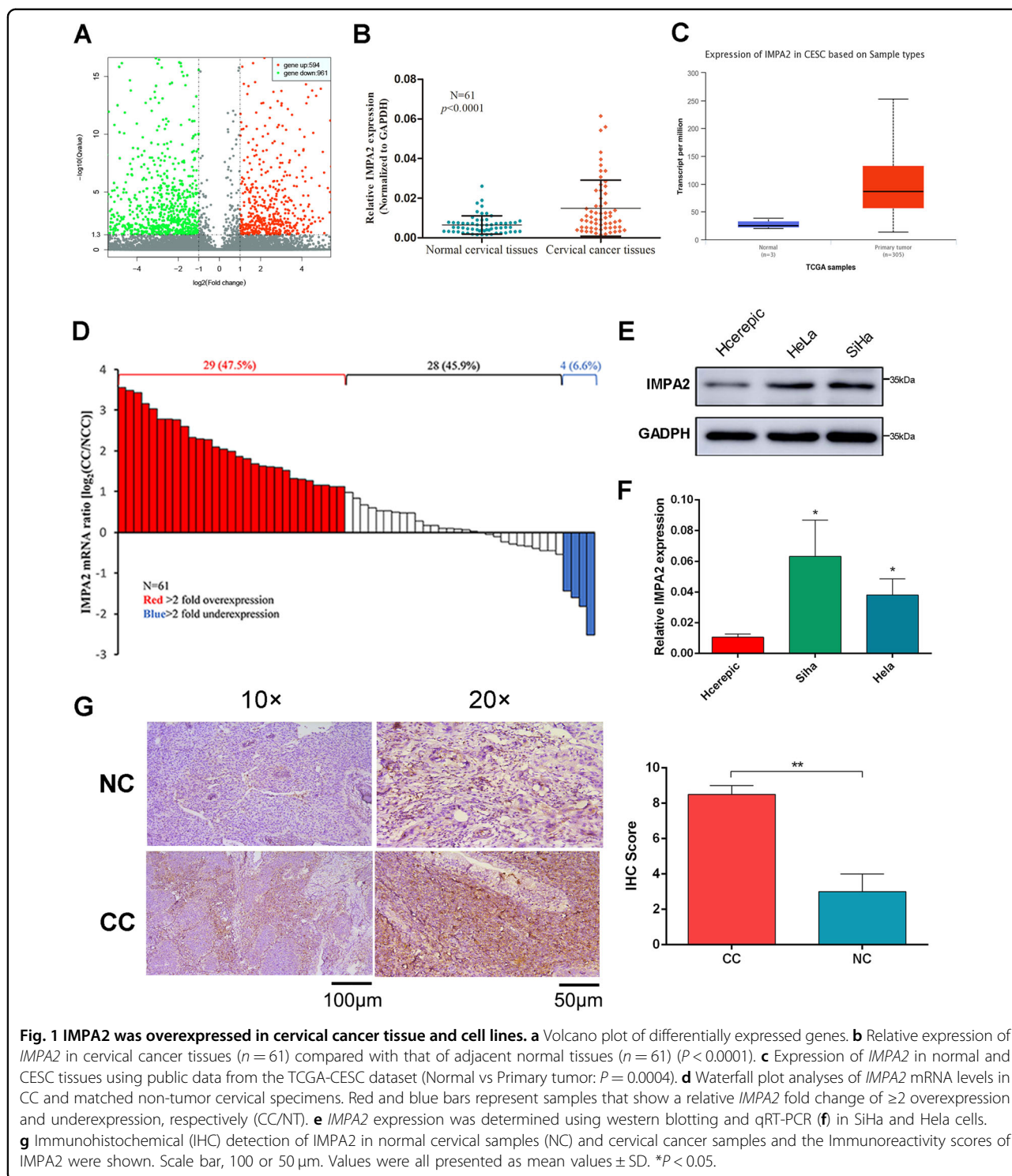
Results

IMPA2 is overexpressed in cervical cancer

Comparing the gene expression profiles of CCIS and adjacent normal cervical samples resulted in 1555 differentially regulated genes at *P* < 0.05. Among the significant genes, 961 genes were up-regulated and 594 were down-regulated in CCIS (Fig. 1a). Of these, *IMPA2* gene was upregulated 11 times. Further real-time PCR was used to determine the *IMPA2* expression pattern in 61 pairs of cervical cancer tissues and their matched adjacent non-tumor cervical tissues. *IMPA2* is significantly overexpressed in cervical cancer samples (*P* < 0.0001, Fig. 1b). Overexpression of more than 2-fold was displayed in 47.5% (29 of 61) of the cervical cancer samples compared with non-tumor samples (Fig. 1d). Analysis of a public CESC (Cervical squamous cell carcinoma) dataset from The Cancer Genome Atlas (TCGA) (<https://tcga-data.nci.nih.gov/tcga/tcgaDownload.jsp>) also showed significant *IMPA2* overexpression (Fig. 1c)²¹. Expression of *IMPA2* was also compared among cervical cancer cell lines and normal cervical epithelial cell line to prove the overexpression (Fig. 1e, f). Moreover, increased protein level of *IMPA2* was also observed in paired cervical cancer samples by immunohistochemistry (IHC; Fig. 1g).

Inhibition of IMPA2 suppresses tumorigenesis of SiHa cells in vivo

SiHa cells infected with *IMPA2* shRNA or shRNA control were subcutaneously injected into each flank of nude mice. The tumor size of each nude mouse was



measured and record weekly to draw the growth curve (Fig. 2b). After 5 weeks, all the mice were anesthetized to perform whole-body fluorescent imaging. As shown in Fig. 2a, no obvious metastasis was discovered in both groups. After that, all the mice were killed to harvest the

xenografts. The tumor size and weight were measured and compared between groups. The *IMPA2* silencing group showed significantly smaller tumor size ($P = 0.0274$) and lighter average weight ($P = 0.0123$) than the control group (Fig. 2c, d).

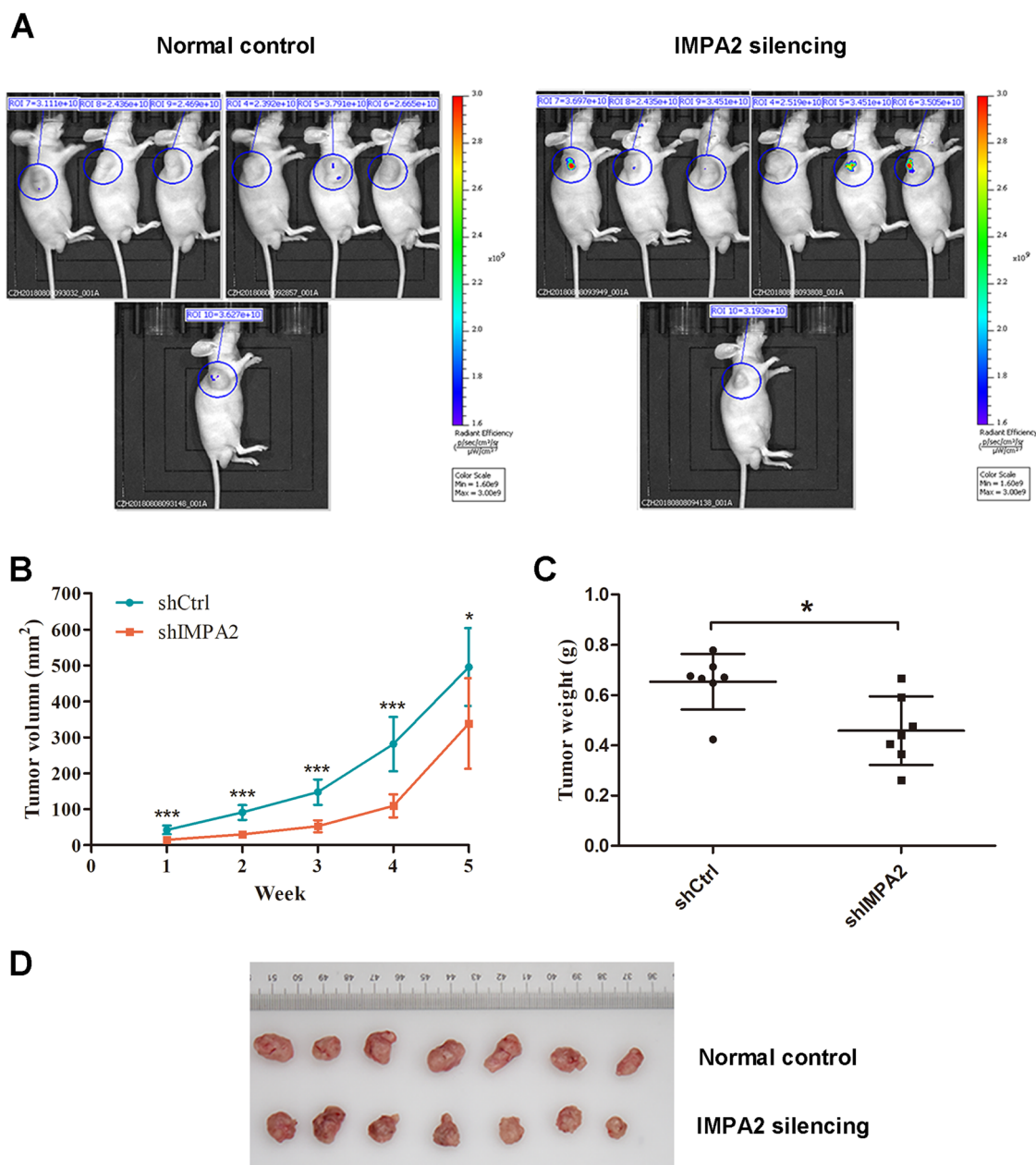
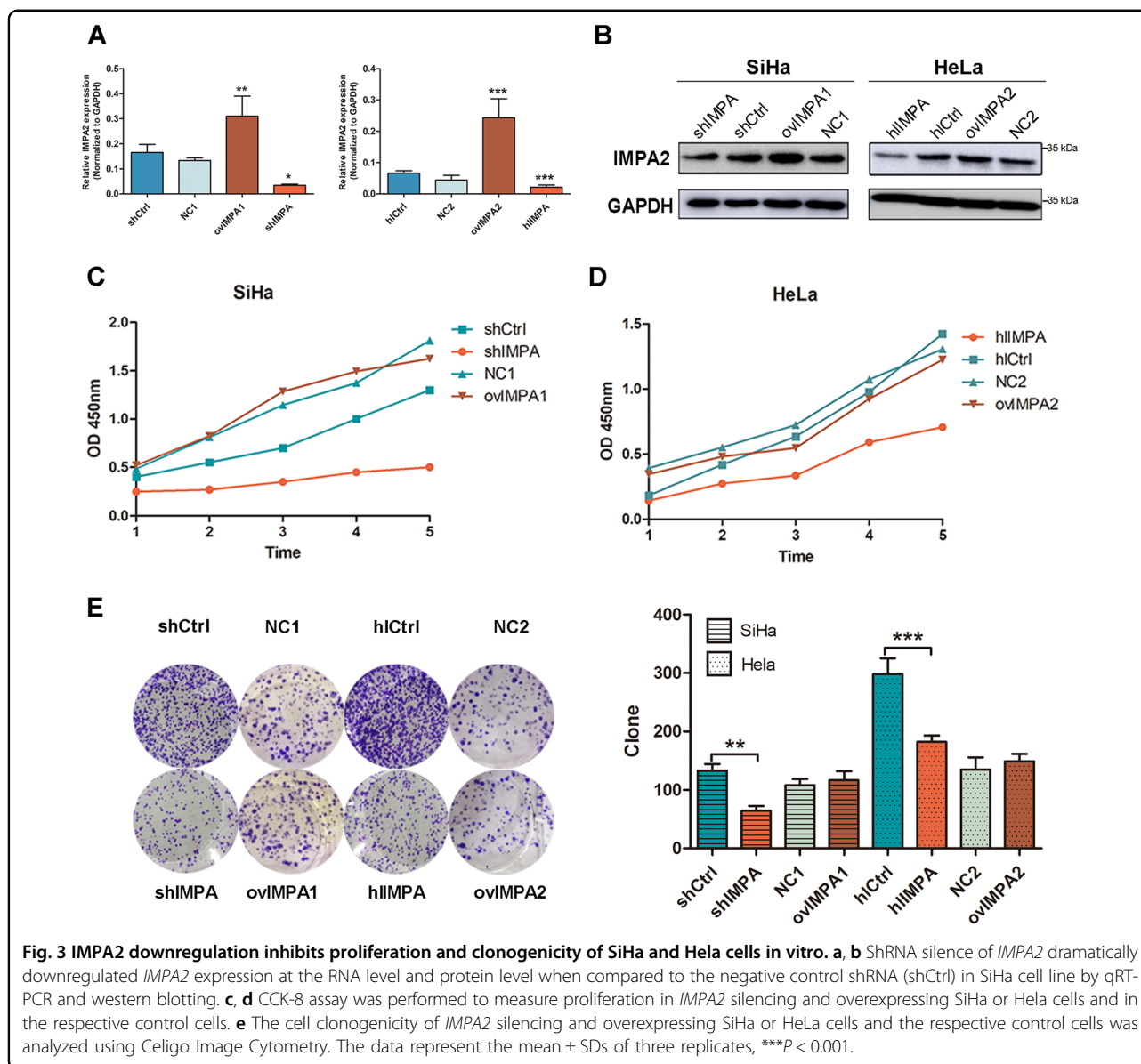


Fig. 2 Inhibition of IMPA2 suppresses tumor growth in vivo. **a** Nude mice were transplanted subcutaneously with SiHa cells transfected with *IMPA2* shRNA or the control shRNA. After 35 days, the mice were killed. Whole-body fluorescent imaging was performed for each nude mouse, and the representative pictures were recorded and presented. **b** Tumor volumes were measured weekly from week one to five post-injection. **c** Tumor weights were measured after the mice were killed. Bars indicate mean values \pm SD. **d** A representative picture of the morphology of tumor xenografts after excision at the 35th day. * $P < 0.05$.

IMPA2 promotes the proliferation and clonogenicity of cervical cancer cells in vitro

The role of *IMPA2* in cervical cancer cells was detected after transfected with overexpressed plasmids and small interfering RNA (siRNA) lentivirus. The downregulation and overexpression efficiency were verified using qRT-

PCR and western blotting (Fig. 3a, b). CCK8 cell viability assay (Fig. 3c, d) and colony formation assay (Fig. 3e) were performed to evaluate cell growth. As a result, silencing *IMPA2* in SiHa and HeLa cells both significantly slowed the cell growth. Overexpression of *IMPA2* failed to enhance the cell growth in both cervical cancer cells.



Similarly, fewer and smaller colonies appeared in cells treated with *IMPA2*-siRNA than those in controls ($P < 0.01$). In contrast, no significant difference was found between the *IMPA2* overexpression group and the control group.

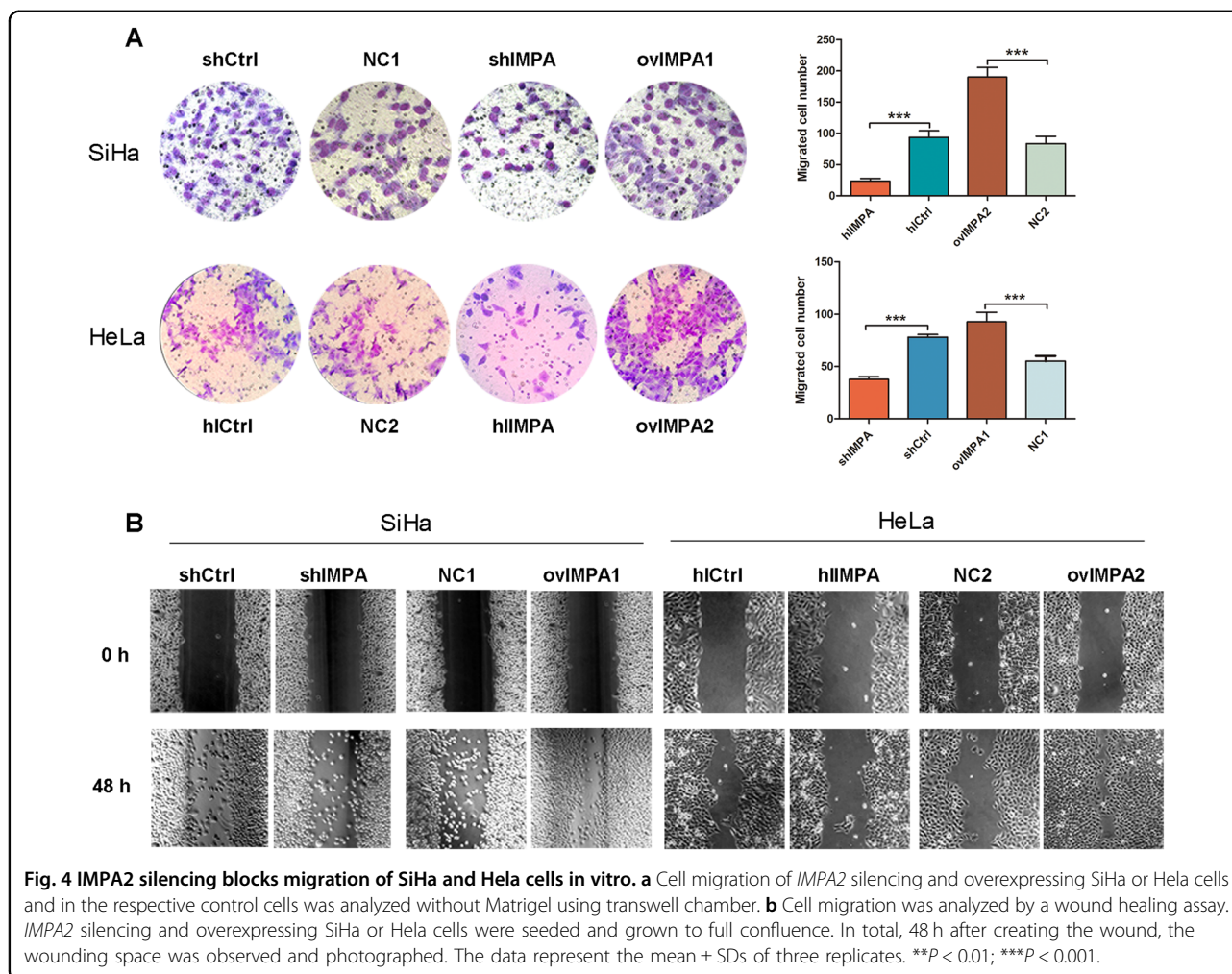
IMPA2 promotes the migration of cervical cancer cells in vitro

Wound-healing assay and transwell migration assay were conducted to examine the effect of *IMPA2* on the migration and invasion of cervical cancer cells. *IMPA2* silencing slowed the speed with which both cervical cancer cells filled the scratch, in comparison to the control in an obvious manner (Fig. 4b). The transwell assays

yielded the similar results ($P < 0.001$, Fig. 4a). On the contrary, the cell migration capacity was improved (Fig. 4b) and the number of invaded cells were significantly higher ($P < 0.001$, Fig. 4a) in *IMPA2* overexpression group.

Pathway analysis of differentially expressed protein between shCtrl and shIMPA2

The proteomic profile of shCtrl and shIMPA2 (Fig. 5) was determined by LC-MS/MS. A total of 4364 proteins were identified. Using a cutoff value 1% FDR for statistical significance, 267 proteins were found to be differentially expressed: 112 significantly overexpressed (shIMPA2/shCtrl ratio ≥ 1.50) and 155 underexpressed

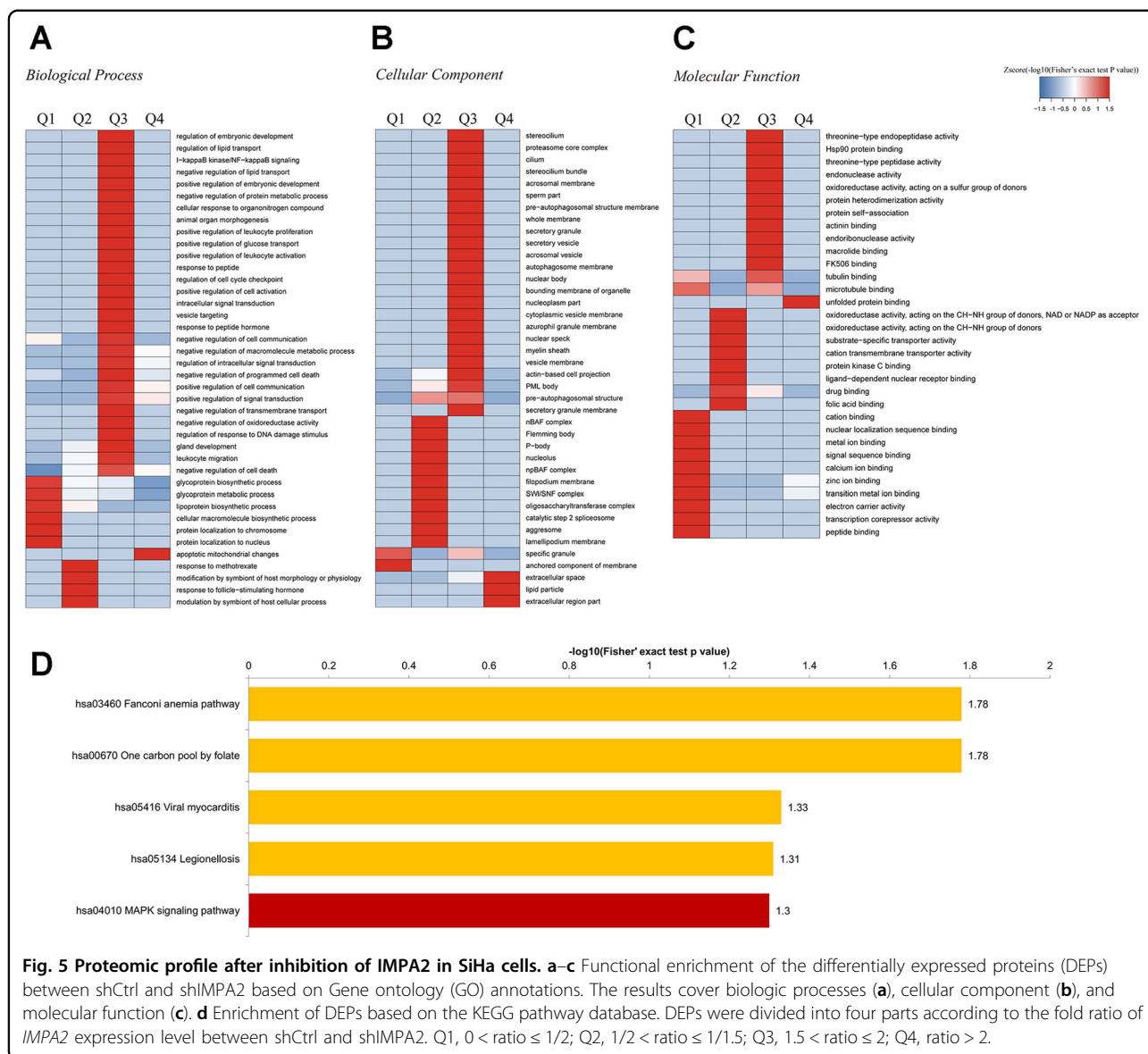


(shIMPA2/shCtrl ratio ≤ 0.50). Further bioinformatics analysis was then performed to assess whether the DEPs were related to specific molecular pathways. In the Gene Ontology (GO) enrichment, 14 biological processes, 8 molecular functions, and 8 cellular components were enriched with statistical significance (Fig. 5a–c). Main biological processes include DNA repair, glycoprotein biosynthesis and metabolism, RNA biosynthesis, and cell death process. The analysis by cellular components showed that *IMPA2* silencing produced a more profound impact on autophagosome-related structure and secretory granule membrane. Moreover, the analysis of molecular functions showed that proteins involved in the binding of transcript, protein kinase and drug, and folic acid, as well as many enzymatic activities like oxidoreductase and DNA polymerase. Cluster analysis based on shIMPA2/shCtrl ratio showed the involved biological processes in more detail (Fig. 5b). KEGG pathway enrichment analysis indicated that most of the DEPs were related to Fanconi anemia pathway, one carbon pool by folate, viral myocarditis, legionellosis,

and MAPK signaling pathway (Fig. 5d). Eight DEPs involved in the MAPK pathway were significantly changed after inhibition of *IMPA2*, including four upregulated proteins (HSPA1L, RAP1A, NFKB1 and TAB1) and four downregulated proteins (MAP2K3, EPHA2, IL1RAP, and ECSIT). The fold change and primary information of these proteins were detailed in Table 2.

Inhibition of *IMPA2* activates the ERK/MAPK pathway

To understand further the mechanisms responsible for *IMPA2*-related cancer progression, MAPK signaling pathways were analyzed by Western blotting based on the proteomic profile results. We found that compared with the shCtrl group, *IMPA2* silencing significantly increased ERK phosphorylation in SiHa and HeLa cells. Total levels of ERK showed no statistical differences. And *IMPA2* had little effect on JNK and p38 phosphorylation (Fig. 6a). Furthermore, silenced *IMPA2* activating ERK expression was also verified in xenografts by immunohistochemical staining (Fig. 6b). Thereafter, ERK inhibitor

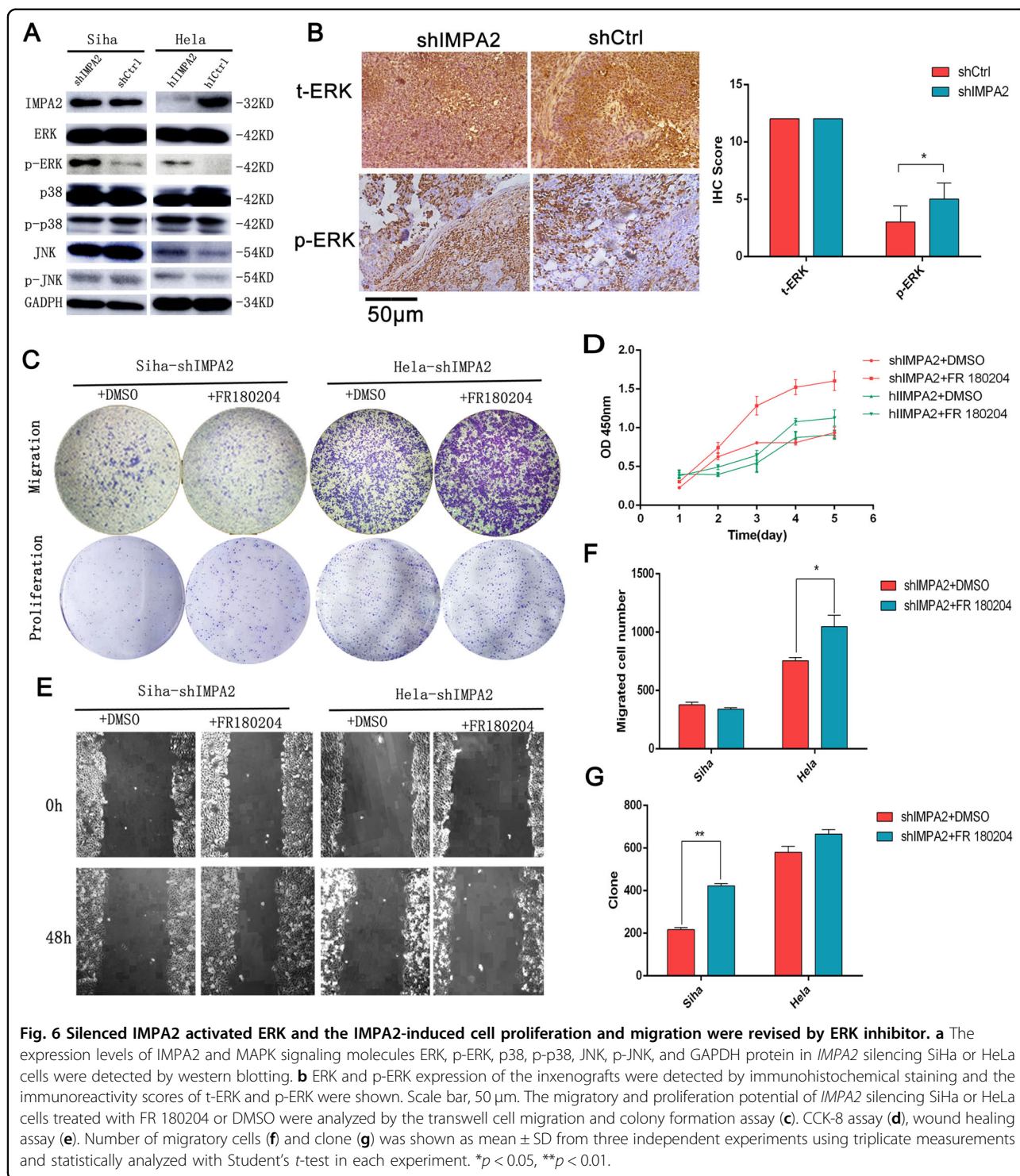


FR180204 (10 μmol) was added in *IMP2*-silenced SiHa and Hela cells for 48 h. We found that FR180204 treatment significantly reversed the *IMP2*-induced decrease in cell viability (Fig. 6d), cell migration and invasion in Hela cell (Fig. 6c, e), suggesting that activation of the ERK signaling pathway may result in inhibitory of proliferation and migration induced by *IMP2* in cervical cancer.

Discussion

Cervical cancer progression is a continuous process from normal cervical to cervical intraepithelial neoplasia (CIN) and finally to cancer. Various molecules were involved^{22–25} besides the key role of human papillomavirus (HPV) infection. *IMP2* gene is a protein-coding gene for myo-inositol monophosphatase⁹. This

monophosphatase is one of the key enzymes in inositol phosphate metabolism and finally convert monophosphate into free inositol through dephosphorylation. *IMP2* is received in many studies to be associated with neuropsychiatric diseases, like schizophrenia²⁶, epilepsy²⁷, bipolar disorder^{11,28,29}, and Huntington's disease^{12,30}. Also, *IMP2* inhibition is accepted as the therapeutic mechanism of lithium in bipolar disorders³¹. However, there is only one published article clearly demonstrated the relationship between *IMP2* expression and cancer progression. Lin et al. recently showed that *IMP2* downregulation constitutes a novel signature for cancer metastasis and poor outcomes in ccRCC¹⁵. On the contrary, our data of RNA sequencing (RNA-seq) showed an obvious upregulation of *IMP2* in cervical cancer.



Therefore, our study investigated its ability to act as an oncogene and the possibility to be a potential diagnostic and prognostic biomarker as well as a therapeutic target in cervical cancer. In the present study, *IMPA2* was upregulated in cervical cancer tissues when compared with pair matched normal tissues, which is consistent

with the dataset of *IMPA2* from TCGA. And about 47.5% (29/61) overexpressed more than 2-fold. However, the upregulation of *IMPA2* failed to correlate with clinical characteristics, HPV types and overall survival.

Our results demonstrated that inhibition of *IMPA2* could slow the proliferation and promote the migration

Table 2 Primary information and fold change of 8 DEPs involved in the MAPK pathway.

Gene name	Protein accession	Protein description	SI/SN ratio
HSPA1L	P34931	Heat shock 70-kDa protein 1-like	2.016
TAB1	Q15750	TGF-beta-activated kinase 1 and MAP3K7-binding protein 1	1.823
RAP1A	P62834	Ras-related protein Rap-1A	1.573
NFKB1	P19838	Nuclear factor NF-kappa-B p105 subunit	1.551
EPHA2	P29317	Ephrin type-A receptor 2	0.644
MAP2K3	P46734	Dual specificity mitogen-activated protein kinase kinase 3	0.64
IL1RAP	Q9NPH3	Interleukin-1 receptor accessory protein	0.587
ECSIT	Q9BQ95	"Evolutionarily conserved signaling intermediate in Toll pathway, mitochondrial"	0.511

SI silenced *IMPA2* group, SN negative control group.

of SiHa and Hela cells (Figs. 3, 4). And this effect of promoting tumorigenesis was also confirmed in vivo (Fig. 2). However, the in vivo result showed no migration or invasion in our shCtrl or sh*IMPA2* group. This can partly explain why *IMPA2* was not associated with clinical and pathological characteristics well (Table S1). And as introduced previously, *IMPA2* was identified upregulated in carcinoma in situ of cervix. We suspect that *IMPA2* can be a promoting element in the early stage of cervical cancer, but the further migration or invasion still need other contributing factors. Collectively, the present study is the first report to demonstrate that *IMPA2* may act as an oncogene in cervical cancer.

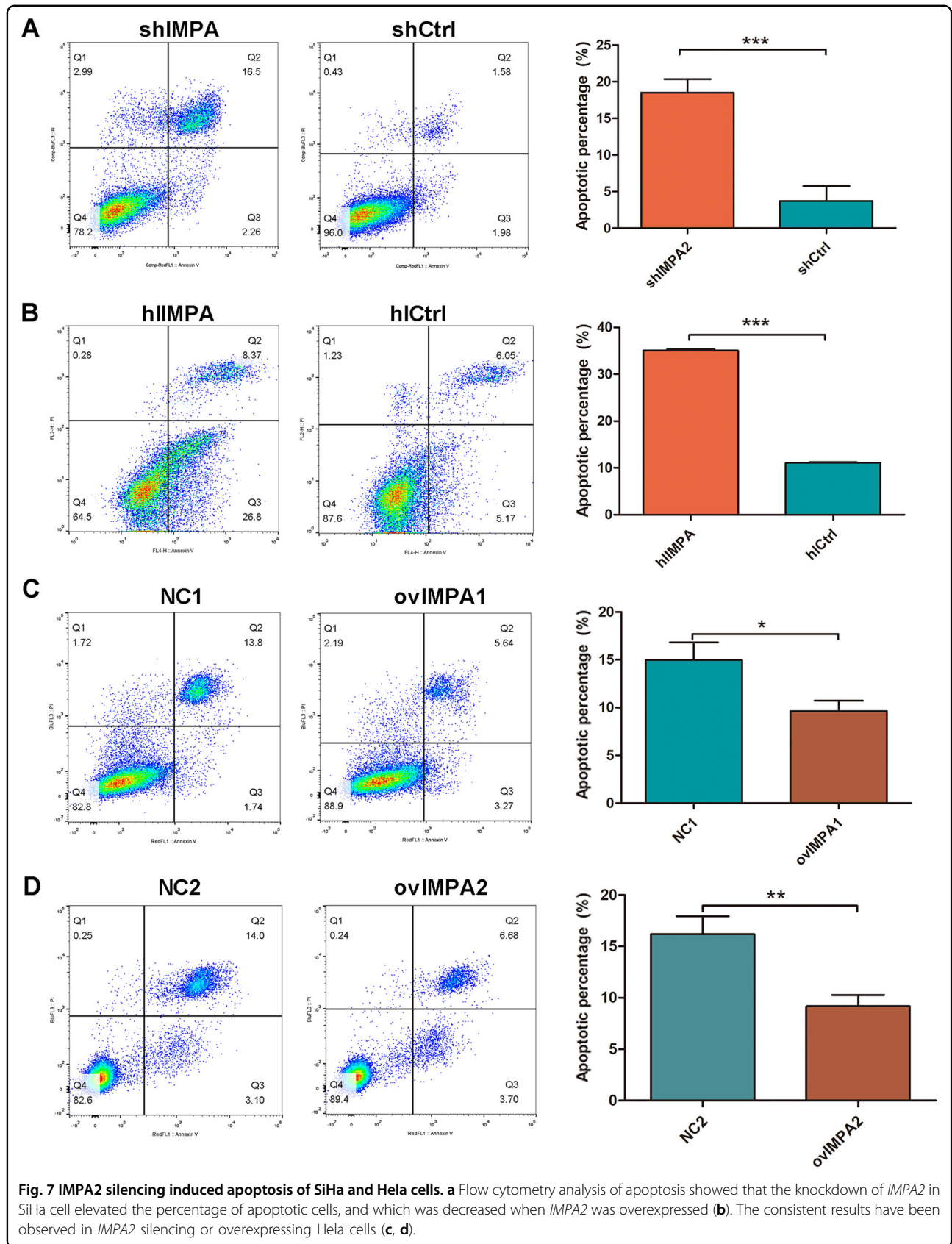
As the mechanism of promoting effect of *IMPA2* has not been studied yet, we first traced back to the researches about mechanisms behind the role of *IMPA2* in neuropsychiatric diseases. Most of the studies agreed that inhibition of *IMPA2* might induce IP3 accumulation and/or inositol depletion, which can finally regulate autophagy to help treat neurodegenerative diseases or bipolar disorders^{12,30,31}. However, the mechanism of *IMPA2* in cancer is utterly unknown. We therefore performed proteomics analysis to look for clues of molecular regulation by *IMPA2* in cervical cancer. In all, 267 proteins with different expression were detected, 149 of which have previously reported to be potentially related to biological processes of DNA damage repair, cell death, glycoprotein biosynthesis and metabolism, RNA biosynthesis, and embryonic development. Clustering analysis showed the involvement of cell death in more detail, as regulation of cell death, programmed cell death, and apoptotic mitochondrial changes were all significantly clustered.

The KEGG enrichment analysis for the identification of pathways unveils possible involvement of MAPK signaling pathway. MAPK plays an important role in regulating cell proliferation³², differentiation^{33,34}, cell cycle arrest³⁵, apoptosis^{24,36,37}, immune function³⁸, and autophagy^{36,39}. The MAPK signaling pathway is shared by four distinct

cascades⁴⁰, including Jun amino-terminal kinases (JNK1/2/3), extracellular signal-related kinases (ERK1/2), p38-MAPK and ERK5. The expression of above key molecules of SiHa and Hela cells pre and post inhibition of *IMPA2* were compared by western blotting. Phosphorylation of ERK was activated after *IMPA2* silencing. JNK 1/2/3 and p38 remained unchanged (Fig. 6), suggesting that MAPK/ERK signaling pathway take part in *IMPA2*-induced tumorigenesis of cervical cancer.

Many researches about chemotherapeutic drugs^{41,42}, tumor-related gene⁴³, microRNA³⁸, and lncRNA⁴⁴ have shown multiple effects on cervical cancer by regulation of MAPK signaling pathway. However, most of the studies agreed that phosphorylation of ERK^{38,45} was upregulated to promote the proliferation or (and) suppress the apoptosis^{33,46} of cervical cancer, while evidences showed contrary effect in this study (Fig. 6). When added ERK inhibitor in *IMPA2*-silenced cells, we could find that the proliferation capacity of Hela and migration of SiHa could not be revised completely (Fig. 6f, g). Therefore, we thought ERK cannot regulate tumorigenesis directly. Previous studies demonstrated that activation of ERK MAPK could also induce cytotoxicity or tumor inhibition in some cancers^{19,41,47}. Some studies revealed that activation of ERK could promote apoptosis progress^{48,49}. And as we all know, apoptosis is a common process of programmed cell death and plays a key role in maintaining cellular homeostasis in normal and cancer cells^{35,50}. Therefore, we suspect that upregulated ERK decreased cervical cancer progression by activating apoptosis in *IMPA2* silencing cells. And the primary apoptosis assay by using flow cytometry had initially verified our hypothesis (Fig. 7), but this hypothesis needs to be confirmed in a further study.

In conclusion, *IMPA2* is a novel tumor promotor that regulates ERK MAPK in cervical cancer. Thus, silencing *IMPA2* could step down proliferation and metastasis of cervical cancer cells. It could also induce activation of



ERK. These findings provided promising insights into developing novel cancer therapies by inhibiting the *IMPA2* in cervical cancer.

Acknowledgements

This work was supported by grants from National Natural Science Foundation of China (81470133), Natural Science Foundation of Hunan Province (2019JJ40426), Fundamental Research Funds for the central Universities of Central South University (2018zzts928), and Hunan Provincial Department of Finance (201895).

Conflict of interest

The authors declare that they have no conflict of interest.

Publisher's note

Springer Nature remains neutral with regard to jurisdictional claims in published maps and institutional affiliations.

Supplementary Information accompanies this paper at (<https://doi.org/10.1038/s41419-020-2507-z>).

Received: 11 February 2020 Revised: 10 April 2020 Accepted: 14 April 2020
Published online: 14 May 2020

References

- Bray, F. et al. Global cancer statistics 2018: GLOBOCAN estimates of incidence and mortality worldwide for 36 cancers in 185 countries. *CA Cancer J. Clin.* **68**, 394–424 (2018).
- Petrosky, E. et al. Use of 9-valent human papillomavirus (HPV) vaccine: updated HPV vaccination recommendations of the advisory committee on immunization practices. *MMWR Morb. Mortal. Wkly Rep.* **64**, 300–304 (2015).
- Duenas-Gonzalez, A. & Campbell, S. Global strategies for the treatment of early-stage and advanced cervical cancer. *Curr. Opin. Obstet. Gynecol.* **28**, 11–17 (2016).
- Marth, C. et al. Cervical cancer: ESMO Clinical Practice Guidelines for diagnosis, treatment and follow-up. *Ann. Oncol.* **28**, iv72–iv83 (2017).
- Ho, G. Y., Bierman, R., Beardsley, L., Chang, C. J. & Burk, R. D. Natural history of cervicovaginal papillomavirus infection in young women. *N. Engl. J. Med.* **338**, 423–428 (1998).
- Wu, Y. et al. Whole-exome and RNA sequencing reveals novel insights into the pathogenesis of HPV associated cervical cancer. *Cancer Biomark* <https://doi.org/10.3233/CBM-190055> (2019).
- Yang, R. et al. Combined transcriptome and proteome analysis of immortalized human keratinocytes expressing Human Papillomavirus 16 (HPV16) oncogenes reveals novel key factors and networks in HPV-induced carcinogenesis. *mSphere* <https://doi.org/10.1128/mSphere.00129-19> (2019).
- Ojesina, A. I. et al. Landscape of genomic alterations in cervical carcinomas. *Nature* **506**, 371–375 (2014).
- Yoshikawa, T., Turner, G., Esterling, L. E., Sanders, A. R. & Detera-Wadleigh, S. D. A novel human myo-inositol monophosphatase gene, IMP18p, maps to a susceptibility region for bipolar disorder. *Mol. Psychiatry* **2**, 393–397 (1997).
- Ohnishi, T. et al. Spatial expression patterns and biochemical properties distinguish a second myo-inositol monophosphatase *IMPA2* from *IMPA1*. *J. Biol. Chem.* **282**, 637–646 (2007).
- Jimenez, E. et al. Genetic variability at *IMPA2*, *INPP1* and *GSK3beta* increases the risk of suicidal behavior in bipolar patients. *Eur. Neuropsychopharmacol.* **23**, 1452–1462 (2013).
- Sarkar, S. et al. Lithium induces autophagy by inhibiting inositol monophosphatase. *J. Cell Biol.* **170**, 1101–1111 (2005).
- Ohnishi, T. et al. Human myo-inositol monophosphatase 2 rescues the nematode thermotaxis mutant *txx-7* more efficiently than *IMPA1*: functional and evolutionary considerations of the two mammalian myo-inositol monophosphatase genes. *J. Neurochem.* **124**, 685–694 (2013).
- French, D. et al. Acquired variation outweighs inherited variation in whole genome analysis of methotrexate polyglutamate accumulation in leukemia. *Blood* **113**, 4512–4520 (2009).
- Lin, Y. F. et al. Dysregulation of the miR-25-*IMPA2* axis promotes metastatic progression in clear cell renal cell carcinoma. *EBioMedicine* **45**, 220–230 (2019).
- Mustafa, D. A. M. et al. T lymphocytes facilitate brain metastasis of breast cancer by inducing Guanylate-Binding Protein 1 expression. *Acta Neuropathol.* **135**, 581–599 (2018).
- Chen, T. P. et al. Increased expression of SKP2 and phospho-MAPK/ERK1/2 and decreased expression of p27 during tumor progression of cervical neoplasms. *Gynecol. Oncol.* **104**, 516–523 (2007).
- Yu, Z. et al. SIX3, a tumor suppressor, inhibits astrocytoma tumorigenesis by transcriptional repression of *AURKA/B*. *J. Hematol. Oncol.* **10**, 115 (2017).
- Wang, Z. et al. The D Domain of LRRC4 anchors ERK1/2 in the cytoplasm and competitively inhibits MEK/ERK activation in glioma cells. *J. Hematol. Oncol.* **9**, 130 (2016).
- Wang, Z. Y. et al. Upregulation of the long non-coding RNA AFAP1-AS1 affects the proliferation, invasion and survival of tongue squamous cell carcinoma via the Wnt/beta-catenin signaling pathway. *Mol. Cancer* **17**, 3 (2018).
- Chandrashekar, D. S. et al. UALCAN: a portal for facilitating tumor subgroup gene expression and survival analyses. *Neoplasia* **19**, 649–658 (2017).
- Chen, S. Q. et al. Analyzing simultaneous positive expression of EZH2 and P53 protein to improve predictive value in cervical squamous cell carcinoma. *Int. J. Gynecol. Cancer* **24**, 1653–1658 (2014).
- Chen, Y. et al. INPP4B restrains cell proliferation and metastasis via regulation of the PI3K/AKT/SKG pathway. *J. Cell. Mol. Med.* **22**, 2935–2943 (2018).
- Xiao, S. et al. Fra-1 is downregulated in cervical cancer tissues and promotes cervical cancer cell apoptosis by p53 signaling pathway in vitro. *Int. J. Oncol.* **46**, 1677–1684 (2015).
- Yadav, S. S. et al. Epigenetic silencing of CXCR4 promotes loss of cell adhesion in cervical cancer. *Biomed. Res. Int.* **2014**, 581403 (2014).
- Li, J. et al. A promoter polymorphism rs2075824 within *IMPA2* gene affecting the transcription activity: possible relationship with schizophrenia. *J. Cell. Mol. Med.* **21**, 658–664 (2017).
- Gurnett, C. A. & Hedera, P. New ideas in epilepsy genetics: novel epilepsy genes, copy number alterations, and gene regulation. *Arch. Neurol.* **64**, 324–328 (2007).
- Tomioka, Y. et al. Association between genetic variation in the myo-inositol monophosphatase 2 (*IMPA2*) gene and age at onset of bipolar disorder. *J. Affect. Disord.* **232**, 229–236 (2018).
- Yoon, I. S. et al. Altered *IMPA2* gene expression and calcium homeostasis in bipolar disorder. *Mol. Psychiatry* **6**, 678–683 (2001).
- Sarkar, S. & Rubinsztein, D. C. Inositol and IP3 levels regulate autophagy: biology and therapeutic speculations. *Autophagy* **2**, 132–134 (2006).
- Sade, Y. et al. IP3 accumulation and/or inositol depletion: two downstream lithium's effects that may mediate its behavioral and cellular changes. *Transl. Psychiatry* **6**, e968 (2016).
- Cuadrado, A. & Nebreda, A. R. Mechanisms and functions of p38 MAPK signalling. *Biochem. J.* **429**, 403–417 (2010).
- Sun, Y. et al. Signaling pathway of MAPK/ERK in cell proliferation, differentiation, migration, senescence and apoptosis. *J. Recept. Signal Transduct. Res.* **35**, 600–604 (2015).
- Ventura, J. J. et al. p38alpha MAP kinase is essential in lung stem and progenitor cell proliferation and differentiation. *Nat. Genet.* **39**, 750–758 (2007).
- Hu, X. et al. Polypeptide fraction from Arca subcrenata induces apoptosis and G2/M phase arrest in HeLa cells via ROS-mediated MAPKs pathways. *Evid. Based Complement. Alternat. Med.* **2015**, 930249 (2015).
- Tan, G. X. et al. PP-22 promotes autophagy and apoptosis in the nasopharyngeal carcinoma cell line CNE-2 by inducing endoplasmic reticulum stress, downregulating STAT3 signaling, and modulating the MAPK pathway. *J. Cell. Physiol.* <https://doi.org/10.1002/jcp.27076> (2018).
- Chiu, C. C. et al. p38 MAPK and NF-kappaB pathways are involved in naphtho [1,2-b] furan-4,5-dione induced anti-proliferation and apoptosis of human hepatoma cells. *Cancer Lett.* **295**, 92–99 (2010).
- Li, Z. H., Li, L., Kang, L. P. & Wang, Y. MicroRNA-92a promotes tumor growth and suppresses immune function through activation of MAPK/ERK signaling pathway by inhibiting PTEN in mice bearing U14 cervical cancer. *Cancer Med.* <https://doi.org/10.1002/cam4.1329> (2018).
- Sui, X. et al. p38 and JNK MAPK pathways control the balance of apoptosis and autophagy in response to chemotherapeutic agents. *Cancer Lett.* **344**, 174–179 (2014).
- Hommes, D. W., Peppelenbosch, M. P. & van Deventer, S. J. Mitogen activated protein (MAP) kinase signal transduction pathways and novel anti-inflammatory targets. *Gut* **52**, 144–151 (2003).

41. Potocnjak, I., Gobin, I. & Domitrovic, R. Carvacrol induces cytotoxicity in human cervical cancer cells but causes cisplatin resistance: involvement of MEK-ERK activation. *Phytother. Res.* **32**, 1090–1097 (2018).
42. Vazhappilly, C. G. et al. Inhibition of SHP2 by new compounds induces differential effects on RAS/RAF/ERK and PI3K/AKT pathways in different cancer cell types. *Investig. New Drugs* <https://doi.org/10.1007/s10637-018-0626-5> (2018).
43. Zheng, H. Y., Shen, F. J., Tong, Y. Q. & Li, Y. PP2A inhibits cervical cancer cell migration by dephosphorylation of p-JNK, p-p38 and the p-ERK/MAPK signaling pathway. *Curr. Med. Sci.* **38**, 115–123 (2018).
44. Liu, X., Yang, Q., Yan, J., Zhang, X. & Zheng, M. LncRNA MNX1-AS1 promotes the progression of cervical cancer through activating MAPK pathway. *J. Cell. Biochem.* <https://doi.org/10.1002/jcb.27712> (2018).
45. Sun, Q., Liang, Y., Zhang, T., Wang, K. & Yang, X. ER-alpha36 mediates estrogen-stimulated MAPK/ERK activation and regulates migration, invasion, proliferation in cervical cancer cells. *Biochem. Biophys. Res. Commun.* **487**, 625–632 (2017).
46. Wang, K. & Zhu, Y. Dexmedetomidine protects against oxygen-glucose deprivation/reoxygenation injury-induced apoptosis via the p38 MAPK/ERK signalling pathway. *J. Int. Med. Res.* **46**, 675–686 (2018).
47. Chen, J. C., Huang, C., Lee, I. N., Wu, Y. P. & Tang, C. H. Amphiregulin enhances cell migration and resistance to doxorubicin in chondrosarcoma cells through the MAPK pathway. *Mol. Carcinog.* **57**, 1816–1824 (2018).
48. Xiong, W. et al. DAPK1-ERK signal mediates oxygen glucose deprivation reperfusion induced apoptosis in mouse N2a cells. *J. Neurol. Sci.* **387**, 210–219 (2018).
49. Zong, D. et al. Notch1 regulates endothelial apoptosis via the ERK pathway in chronic obstructive pulmonary disease. *Am. J. Physiol. Cell Physiol.* **315**, C330–C340 (2018).
50. Nass, J. & Efferth, T. Insights into apoptotic proteins in chemotherapy: quantification techniques and informing therapy choice. *Expert Rev. Proteomics* **15**, 413–429 (2018).